5
Limiting Factors: Operating Conditions of the Receiver and Thermally Induced Flow Instabilities

It may be concluded from the previous chapter that the chances of failure of an open volumetric air receiver due to the dust deposition may be mitigated by using a cleaning and dust-collection device during its operation. Thus, the cyclone separator is selected based on a comparative assessment for the designed receiver. The cyclone separator will consume an additional power corresponding to its pressure-drop. Including the parasitic losses due to the receiver internals, the efficiency of an air receiver will be reduced. A literature review infers the need of a dedicated correlation for estimating the pressure-drop across the designed absorber; [see e.g. Edouard *et al., (*2008)]. This is certainly a limiting factor for achieving a high efficiency at the desired operating condition in arid deserts. The experiments and simulations are performed to address the same and are presented in the sub-section 5.1 of this chapter.

Literature review also reveals another major challenge or limiting factor associated with the operation of an open volumetric air receiver viz. the thermally induced flow instability [Kribus *et al.*, 1996; Pitz-paal *et al.*, 1997; Fend *et al.*, 2005; Becker *et al.*, 2006]. A brief review on this topic is provided in Chapter 2. Here, the same is extended and some of the findings/observations are highlighted. Fend *et al.* (2005) and Becker *et al.* (2006) reported the existence of a critical heat flux for the onset of flow instability. The effect of thermal conductivity on the flow stability is also reported in Becker *et al.* (2006) and in Sharma *et al.* (2015a, b). Therefore, it is concluded that the undesirable occurrence of flow instability will limit the operating condition as well. This aspect is dealt in the sub-section 5.2 of this chapter.

To investigate the above-mentioned limiting factors, this chapter provides (a) the required pressure-drop correlation across a cylindrical absorber, (b) the deduced correlation for thermal efficiency of open volumetric air receiver and its limitation, (c) an application of the overall efficiency to determine the operating condition of the receiver including a cyclone separator (d) the effect of dust deposition on the operating condition of receiver and finally (e) the flow stability analysis in the designed receiver using theoretical and numerical approach.

5.1 OPERATING CONDITION

This subsection deals with the deduction of operating conditions of an open volumetric air receiver integrated with cleaning device, which is necessary for arid deserts. The subsequent discussion starting with the estimation of pressure-drop leads to the same.

5.1.1 Pressure-Drop: Receiver with Cyclone Separator

The pressure-drop is a result of air flow in the receiver or vice versa. A high pressure-drop demands a large capacity of blower and reduces the system performance. It must be accentuated that all the sub-components of a receiver contribute to this parasitic loss as illustrated in Figure 1.8 (Chapter 1) in addition to a cyclone separator. The estimation of the same is presented in the following sub-sections:

5.1.1.1 Cylindrical Absorber

The absorbers used in open volumetric air receiver are made of metals, alloys and ceramics that are of foam or straight pore -type. The straight pore based absorbers provide low pressure-drop and are less prone to the dust deposition. However, the porosity is generally lower than the foam-type due to manufacturing constraints. There are a number of correlations to predict the pressure-drop (Δp) across the foam-type absorbers [see e.g. Ergun, 1952; Innocentini *et al.*, 1999; Lacroix *et al.*, 2007]. In straight pores, the Hagen-Poisseuille (HP) equation may be preferred for a better estimation of Δp assuming the fully developed laminar flow conditions. These are listed in Table 5.1 as eq. (5.1) in which the inclusion of minor loss with HP accounts for the sudden contraction/expansion at the inlet/outlet of absorber [White, 2011]. For a pore length which is comparable to that of the developing region, the presented correlations for estimating Δp by Holmes (1967), Astarita & Greco (1968) and Sherman (1992) are compared. A visibly wide variation between these correlations confirms the need of a dedicated correlation for the specialized absorber geometry.

Table 5.1: Expressions for the pressure-drop estimation across an absorber.

Absorber pore type	Equation	Expression
Foam	Ergun (1952)	$\frac{\Delta p}{L}=\frac{150\mu_f(1-\varepsilon)^2u_f}{d_{pore}^2\varepsilon^3}+\frac{1.75\rho_f(1-\varepsilon)u_f^2}{d_{pore}\varepsilon^3}$
	Innocentini *et al.*, (1999)	$\frac{\Delta p}{L}=\frac{66.67\mu_f u_f}{d_{pore}^2}+\frac{1.17\rho_f u_f^2}{d_{pore}\varepsilon^2}$
	Lacroix *et al.*, (2007)	$\frac{\Delta p}{L}=\frac{66.67\mu_f(1-\varepsilon)^2u_f}{d_s^2\varepsilon^3}+\frac{1.17\rho_f(1-\varepsilon)u_f^2}{d_s\varepsilon^3},\ d_s=\frac{d_{pore}[4/3\pi(1-\varepsilon)]^{1/2}}{1-[4/3\pi(1-\varepsilon)]^{1/2}}$
Straight	Hagen-Poiseuille (HP) + minor loss (White 2015)	$\frac{\Delta p}{L}=\frac{32\mu_f \mathrm{v}_p}{d_{pore}^{\ 2}},\ \Delta p_{\mathrm{minor}}=\frac{1}{2}\rho_f \mathrm{v}_p^2\left[\left(1-\frac{A_{np}}{A_{pore}}\right)^2+0.42\left(1-\frac{A_{np}}{A_{pore}}\right)\right]$ (5.1)
	Sherman (1992)	$\Delta p=\frac{32\mu_f \mathrm{L}\mathrm{v}_p}{d_{pore}^{\ 2}}+m\frac{1}{2}\rho_f \mathrm{v}_p^2,\ m=2.28$
	Holmes (1967)	$\Delta p=\frac{1}{2}\rho_f \mathrm{v}_p^2\left(K+K'/\mathrm{Re}\right),\ K=2.24,\ K'=38.3$
	Astarita & Greco (1968)	$\Delta p=\frac{795}{\mathrm{Re}}\frac{\rho_f \mathrm{v}_p^2}{2}$ for $\mathrm{Re}\le 146$, $5.48\frac{\rho_f \mathrm{v}_p^2}{2}$ for $\mathrm{Re}>146$

Here, L is the length of absorber, μ_f is the dynamic viscosity of fluid, ρ_f is the density of fluid, ε is the porosity of absorber, u_f is the superficial speed, d_{pore} is the pore diameter or an equivalent foam characteristics, d_s is the strut diameter of foam, v_p is speed of fluid in pore, A_{np} is the total flow area of absorber and A_{pore} is the pore cross-section. Experiments are also performed to measure Δp across the straight pore based cylindrical absorber at different mass flow rate ($\dot{m}$) of air under ambient conditions. The schematic of experimental setup is shown in Figure 5.1(a), which consists of a blower, two connecting pipes each of length ~0.83 m, an absorber of length (L) ~0.0254 m, pore diameter (d_{pore}) ~0.002 m and porosity (ε) ~ 52%, a differential pressure transducer (DPT: Dwyer 475 mark III with an accuracy of ca. ±1.5%, a rotameter and a hot-wire anemometer (Fisher scientific make with an accuracy of ca. ±1%). One of the fabricated brass absorbers with the circular pores is depicted in Figure 5.1(b). The blower maintains the required $\dot{m}$ of air and the installed DPT measures Δp across the absorber. The $\dot{m}$ is controlled with a valve and is measured using the installed rotameter. The experiments were repeated three times for each of the $\dot{m}$ wherein an uncertainty of ca. ±2 Pa is recorded. The average value of the measured Δp is finally adopted for analysis. A comparison between the

rotameter and the hot-wire anemometer based $\dot{m}$ values showed an uncertainty of ca. 5%. The measured and calculated pressure-drop with respect to the pore diameter based Reynolds number $Re_p = m'' d_{pore}/\mu_f$ with m'' as the mass-flux is shown in Figure 5.2. This depicts that the measured values of Δp are in between the straight pore (HP) and the foam-type absorber based expressions. As expected, the foam-type absorber based correlations substantially over-predicts Δp and is inferred from the effect of tortuosity with such an absorber. Moreover, there is a significant variation among the predicted values of correlations. The HP equation with/without minor losses under predicts Δp and the deviation increases with Re_p. These may be attributed to the (a) fully developed flow region given by the development length ($L_d/d_{pore} \sim 0.06 Re_p$) and (b) inadequacy of estimating the minor losses [White, (2011)]. All the considered correlations for developing laminar flow, except Sherman (1992), either over or under predicts Δp and the deviation increases with pore diameter based Reynolds number ($Re = \rho v d_{pore}/\mu$). Besides, this correlation depends on the dimensional parameters such as fluid property that may be a limiting factor being temperature dependent and for analyzing the possible flow instability in an absorber pore at a high temperature. Thus, the findings are consistent with Edouard *et al.* (2008) and the need of a realistic correlation to estimate Δp based on the non-dimensional parameters such as *Re* for air with $Pr \sim 1$ across the straight-pore based cylindrical absorber is realized. Further, this may be adopted for the similar straight pore type absorbers with some relevant corrections and even applied for the desired non-isothermal conditions. To complement these analyses, a detailed three-dimensional numerical analysis is performed using Fluent 13.0 with the described numerical setup in Table 5.2. The continuity and momentum equations as in are solved at the steady-state. Here, $\vec{V}$ is the velocity of air, p is the static pressure, ρ_f is the density and ν_f is the kinematic viscosity of fluid viz. air.

Table 5.2: Setup for three dimensional numerical simulations.

Mesh-type	Resolution (mm)	Equations	Convergence
Polyhedra	Mesh 1: 1.25mm Mesh 2: 1mm **Mesh 3: 0.75mm** Mesh 4: 0.5mm	Continuity, Momentum	10^{-5} - 10^{-6}

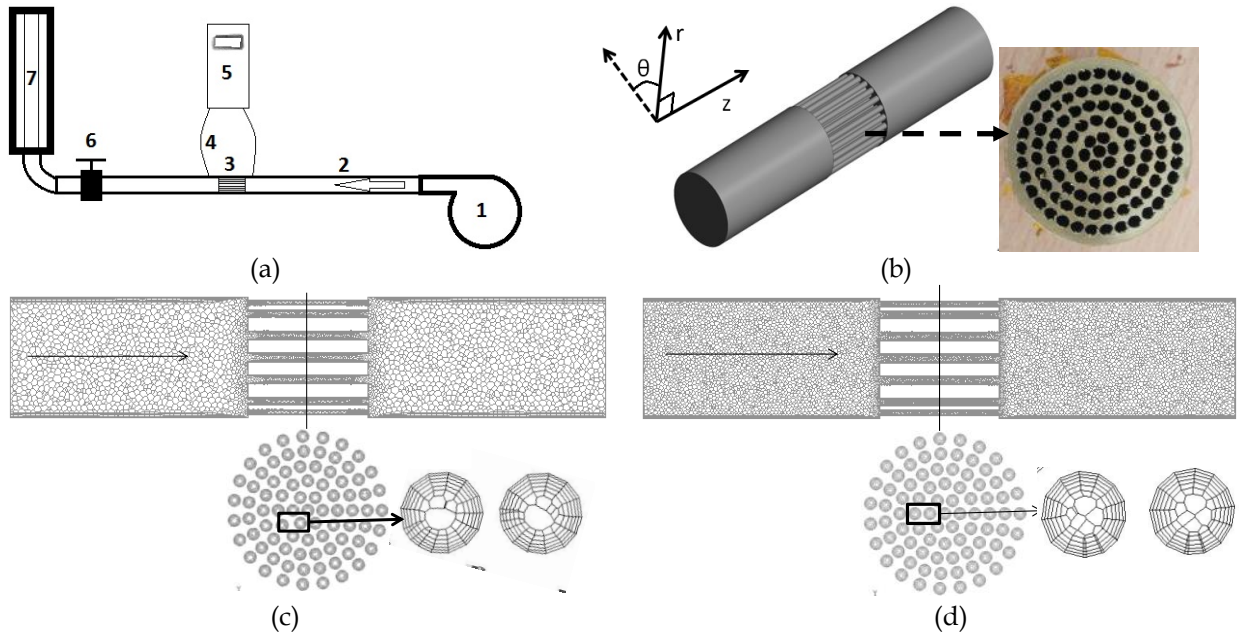

Figure 5.1: (a) Schematic of experimental setup showing 1:blower, 2:pipe, 3:absorber, 4-5:DPT with probes, 6:valve, 7:rotameter; (b) modeled geometry and a fabricated brass absorber; (c,d) the generated coarse and fine mesh.

The modeled three-dimensional geometry as in experiment is depicted in Figure 5.1(b). It consists of a straight pipe in which an absorber is placed at the middle and all the pores are physically modeled. The pipe is used to mitigate the effect of inlet and outlet on the Δp across the absorber, as far as possible. Moreover, the effect of inlet and outlet to absorber is included by replicating the experiment. The employed wall-resolved coarse and fine polyhedral mesh along the length and at a cross-section are shown in Figure 5.1(c) and (d). Finally the mesh 3 with an element size of 0.75 mm is selected as depicted in Figure 5.1(d). This is based on a grid independence study in which mesh sizes 1-4 are varied between 1.25-0.5 mm as summarized in Table 5.2. It must be noted that the flow inside a pore is laminar and that the selected mesh should suffice to capture the fully developed axial-velocity profile. A uniform velocity at the inlet to the domain, the zero gage-pressure at the outlet of the domain and no-slip on the walls are applied as the boundary conditions. Therefore, the adopted numerical setup may provide a reasonable value of Δp.

The numerically analyzed Δp at the same Re_p as in experiment is compared with its measured values in Figure 5.2. It may be noted that the performed simulation also includes SST turbulence model in order to assert or capture, to some extent, the effect of inlet disturbances, if any, on the pressure-drop. The maximum uncertainty of ca. *~10%* is included for the recorded variation of ca. ±2 Pa in addition to 5% uncertainty in flow-rate measurement. It is obvious that the measured and the calculated values of Δp follow the same trend with an over-prediction of ca. 10-25% in simulation. This is conservative and thus, adaptable in view of practical considerations. Furthermore, the SST model based simulations compare well to that of the laminar flow condition inferring the negligible effect of inlet turbulence. The computed values are the closest to the measurement in comparison to the provided expressions. As the next step, Δp is numerically obtained for the absorbers with $0.32 \leq \varepsilon \leq 0.62$. It is inferred from Figure 5.2 that Δp depends on Re_p and is comparable for the different porosities (ε). Subsequently, using a power-law based curve fitting, a correlation as in eq. (5.2) is derived for Δp across the considered cylindrical absorber; see Figure 5.1(b). Because the developed three-dimensional model replicates experiment setup the influence of jet and disturbance at the inlet is expected to be addressed. The deduced correlation in eq. (5.2) for Δp in terms of Re_p includes the effect of fluid and flow properties and is analyzed for $175 \leq Re_p \leq 600$. This correlation may be adopted for such straight pore type absorbers with minor correction based on experiment or analysis. Recently, the analysis of developed correlation has revealed its capability to predict Δp at a high temperature, as desired, and described in section 5.2.

$$\left.\begin{aligned} \Delta p &= K_p \times \frac{\rho_f \mathrm{v}_p^2}{2} \\ K_p &\approx 179.25 Re_p^{-0.588} \end{aligned}\right\} \tag{5.2}$$

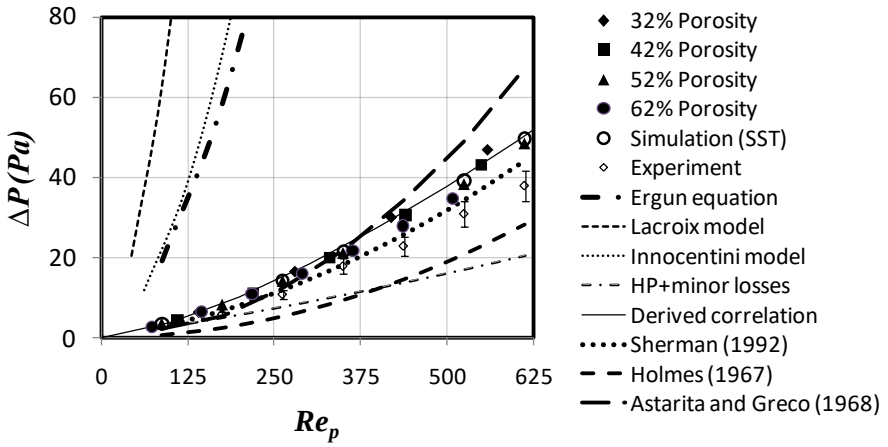

Figure 5.2: A comparison between the measured and the analyzed pressure-drop across an absorber.

5.1.1.2 Effect of Dust Deposition on Pressure-drop

As already explained in chapter 3, the deposition of dust in absorber pores leads to a local or a wide-area temperature rise. This assumes a uniform thickness of the deposited dust layer throughout the length of a pore as illustrated in Figure 5.3 wherein Δp is independent of the radial position in an absorber at a given suction. Thus, the mass flow rate of air in a partly blocked pore ($\dot{m}_{bl}$) will be lower than that of a clean pore ($\dot{m}_{cl}$) and are related as follows:

$$\frac{\Delta p_{cl}}{\Delta p_{bl}} = \frac{\left(179.25 Re_p^{-0.588} \times \frac{\rho_f V_p^2}{2}\right)_{cl}}{\left(179.25 Re_p^{-0.588} \times \frac{\rho_f V_p^2}{2}\right)_{bl}} = 1 \quad \Rightarrow \frac{\dot{m}_{bl}}{\dot{m}_{cl}} = \left(\frac{d_{bl}}{d_{cl}}\right)^{2.42} \left(\frac{\nu_{f\_cl}}{\nu_{f\_bl}}\right)^{0.42} \left(\frac{\rho_{f\_bl}}{\rho_{f\_cl}}\right)^{0.29}. \tag{5.3}$$

The eq. (5.3) shows that mass flow rate of air depends on (a) fluid properties and (b) the hydraulic diameter of a pore. The reduction of mass flow rate in a partly blocked pore is obvious with the first exponent at the right hand side of this equation. This important basic analysis underlines the need of a cleaning device while operating an open volumetric air receiver in arid deserts. The required operating conditions for the same using the required expressions/correlations of pressure-drop are presented subsequently.

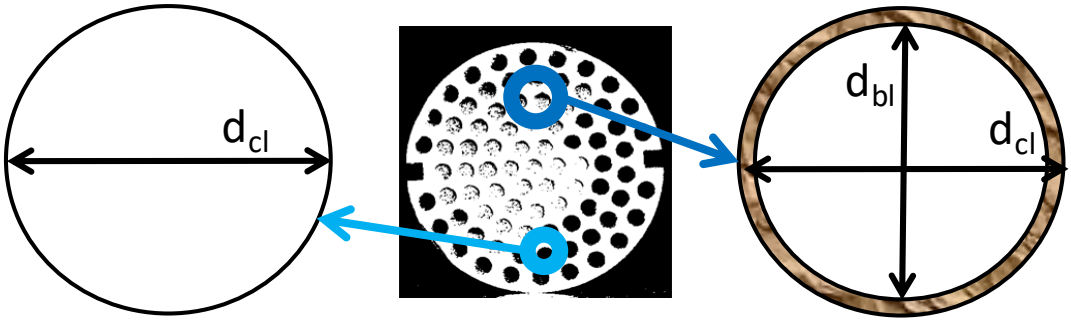

Figure 5.3: The cross-section of a pore without and with a uniform dust layer.

5.1.1.3 Pressure-Drop: Open Volumetric Air Receiver

In addition to the porous absorber, an open volumetric air receiver includes the foot-piece, the perforated plate and the nozzle as explained in Chapter 1. For the designed straight pore based absorber, a correlation for the pressure-drop coefficient is already derived in section 5.1.1. Generally, for the foam type absorbers, the widely employed Ergun equation is presented in Table 5.3. Also, the proposed cyclone separator in Chapter 3 will be installed with the receiver. The pressure-drop in all these individual elements is estimated as in Table 5.3.

Table 5.3: Pressure-drop correlations for the sub-components of an open volumetric air receiver.

Component	Source	Correlation
Absorber (foam)	Ergun (1952)	$\frac{\Delta p}{L} = \frac{150\mu(1-\varepsilon)^2 u_f}{D_p^2 \varepsilon^3} + \frac{1.75\rho(1-\varepsilon)u_f^2}{D_p \varepsilon^3}$
Foot-piece	Darcy-Weisbach Equation (White 2015)	$\Delta p = \frac{\rho_f f L}{D} \cdot \frac{V^2}{2}$

Perforated plate	Holt *et al.*, (2011)	$\Delta p = K_{lp}\frac{\rho_f V^2}{2}$ $K_{la} = 1-2(A_p/A_H)+2(A_p/A_H)^2(1-1/\alpha+1/2\alpha^2)$ $K_{lp} = (2.9-3.79\varphi+1.79\varphi^2)\,\mathrm{K}_{la}$ if $\varphi \le 0.9$ $K_{lp} = (0.876+0.069\varphi)\,\mathrm{K}_{la}$ if $\varphi > 0.9$ $\varphi = (t/d)(A_H/A_P)^{0.2}$
Nozzle	White (2015)	$\Delta p = k.\frac{\rho_f V^2}{2}$ where k= 0.04
Cyclone separator	(See Chapter 4)	$\Delta p = K.\frac{\rho_f V_i^2}{2}$ $K = 1.0213\frac{(\nu/\nu_\infty)^{-0.605}(0.106\,\mathrm{e}^{0.013D_c}\ln \mathrm{V}_i+3.4)}{(\rho/\rho_\infty)}$

5.1.2 Assessing an Open Volumetric Air Receiver for Arid Desert Conditions

The thermal efficiency of an open volumetric air receiver is based on their design and the material properties. This section prescribes an approach for deducing the operating condition of such a receiver with a cyclone separator.

5.1.2.1 Performance of an Open Volumetric Air Receiver

The thermal efficiency of an open volumetric air receiver is defined as the ratio of useful heat gain rate by air to the incident power-on-aperture ($\dot{q}$) as follows:

$$\eta_{th} = \frac{\dot{m}_a c_p (T_{out} - T_o)}{\dot{q}}. \tag{5.4}$$

A comparative assessment of the thermal efficiency with respect to $\dot{q}/\dot{m}_a$ as in Figure 5.4(a) illustrates the substantial variations beyond 700 kJ/kg. Here, the reported data from literature is considered [Fend, 2010; Ávila-Marín *et al.*, 2014; Hoffschmidt *et al.*, 2003]. These are attributed to the different absorber designs and operating conditions. However, all of them show a trend of decreasing thermal efficiency with the increasing $\dot{q}/\dot{m}_a$. This parameter is widely utilized for assessment of a receiver and thus, retained as standard. Therefore, the thermal efficiency is approximated as a function of porosity and $\dot{q}/\dot{m}_a$. Some of these data and the least square method are used for deducing the correlation for thermal efficiency as follows:

$$\eta_{th} = 0.99\left(\frac{\dot{q}}{\dot{m}_a}\right)^{-0.08}(1-\varepsilon)^{-0.34}. \tag{5.5}$$

The derived correlation as in eq. (5.5) is compared with the remaining measured data for a qualitative and a quantitative uncertainty estimation as depicted with a limit of ±10% in Figure 5.4(b) and therefore, it is employed for further evaluation. It is also inferred from Figure 5.4(a) that the available data for $\dot{q}/\dot{m}_a$ > 700 kJ/kg is insufficient and therefore, the need for more experiments is concluded to improve this expression. Hence, the applicability of the derived correlation is currently limited to a $\dot{q}/\dot{m}_a \le$ 700 kJ/kg, which may be considered as one of its limitations.

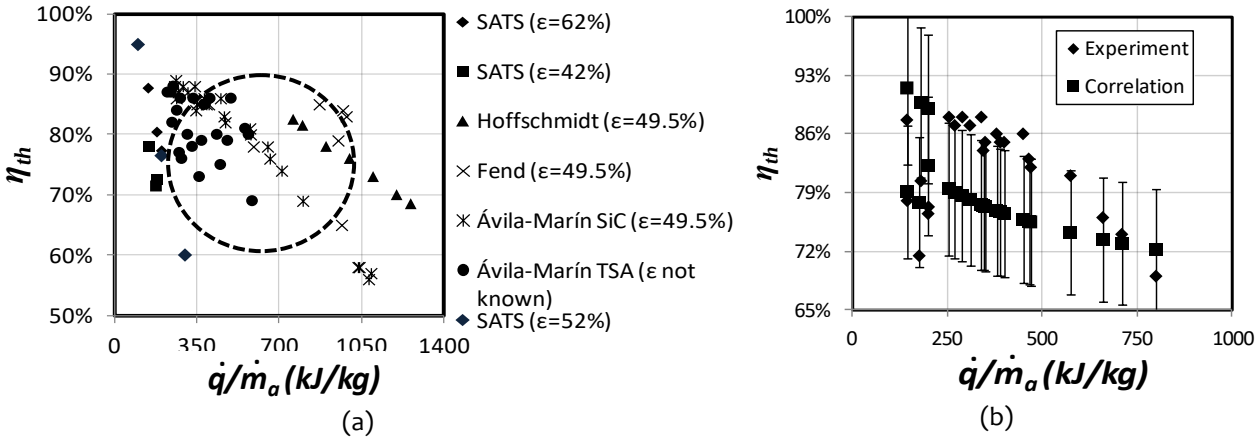

Figure 5.4: A comparison between (a) the measured thermal efficiency, and (b) correlation based and the measured efficiency (%) of the receiver.

5.1.2.2 The Operating Conditions of an Open Volumetric Air Receiver

The thermal efficiency of a receiver describes its heat transfer effectiveness that excludes the effect of parasitic loss offered by the sub-systems including cyclone separator. To incorporate the same, the definition of overall efficiency is proposed for an open volumetric air receiver as follows:

$$\eta_{ov} = \left(\frac{\eta_{th} \times \dot{q}}{\dot{q} + \Delta p_o \times \dot{Q}} \right) = \left(\frac{\eta_{th} \times (\dot{q}/\dot{m}_a)}{(\dot{q}/\dot{m}_a) + \Delta p_o / \rho} \right). \tag{5.6}$$

In this equation the power requirement as a result of the total pressure-drop (Δp_o) is added to the power-on-aperture. To deduce an acceptable operating condition for such a receiver in arid-desert regions a new parameter called *efficiency ratio* ($\eta_r = \eta_{ov}/\eta_{th}$) is introduced. A higher value of η_r implies a lower parasitic loss and vice versa.

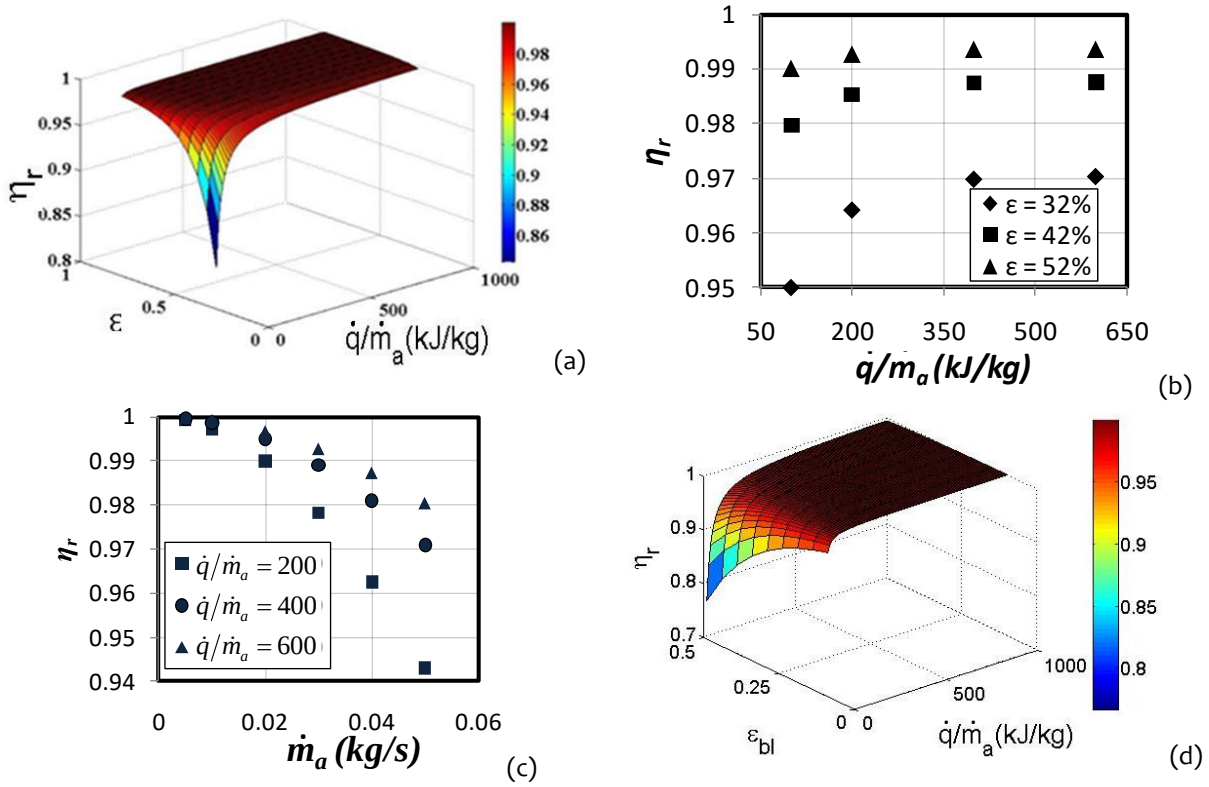

Figure 5.5 Efficiency ratio (η_r) variation for clean receiver with (a) porosity and $\dot{q}/\dot{m}_a$, (b) mass flow rate of air ($\dot{m}_a$) and, η_r variation for partly blocked receiver with (c) mass flow rate of air ($\dot{m}_a$), (d) porosity and $\dot{q}/\dot{m}_a$.

The variation of η_r with respect to $\dot{q}/\dot{m}_a$ and ε is given in Figure 5.5(a). It is affirmed that η_r increases with increase in $\dot{q}/\dot{m}_a$ and ε. The computed values of η_r are compared against the porosity and $\dot{q}/\dot{m}_a$ for $\dot{m}_a$ of 0.01 kg/s in Figure 5.5(b). Here, the pressure-drop across an absorber is conservatively estimated using the Ergun equation, which is the worst possible scenario. This figure reveals that for $\dot{q}/\dot{m}_a$ < 200 kJ/kg the overall efficiency of the presented receiver is notably affected by Δp_o. The highest porosity offers the lowest Δp_o at a given $\dot{m}_a$ and therefore, η_r is the highest. Hence, a high value of $\dot{q}/\dot{m}_a$ and ε are desirable for operating an open volumetric air receiver with a cyclone separator. These values may vary with the scale-up and is a matter for future investigation. In Figure 5.5(c), the variation of η_r is analyzed for $200 \leq \dot{q}/\dot{m}_a \leq 600$ kJ/kg in which $\dot{m}_a$ is varied at a fixed $\dot{q}$ of 5 kW and ε of 52%. Thus, the effect of $\dot{m}_a$ is analyzed in isolation. The obvious reduction in η_r with increasing $\dot{m}_a$ is attributed to Δp_0 and the trend is the same for all cases. The highest value of η_r for $\dot{q}/\dot{m}_a$ of 600 kJ/kg depicts the lowest influence of Δp_o and vice versa. Thus, the need of a high $\dot{q}/\dot{m}_a$ is re-confirmed. Further analyses are performed with the partially blocked absorber in which the blockage (ε_{bl}) is limited up to 50% as an extreme condition. This will enhance the parasitic loss and thus the overall efficiency will further decrease as illustrated in Figure 5.5(d). In addition, the absorber temperature will increase, which is detrimental for a sustained operation. Therefore, operating such a receiver at a high $\dot{q}/\dot{m}_a$ will be of dual advantage in arid-desert regions including a cleaning system for the dust removal. Based on these observations, it is recommended that a porosity (ε) ≥ 50% and a $\dot{q}/\dot{m}_a \geq 200$ kJ/kg may be adopted for operating an open volumetric air receiver with a cyclone separator in arid deserts. The reported findings are likely to be helpful in such regions worldwide. One question remains, whether these operating conditions ensure a stable operation of the receiver? This is answered in the subsequent analysis of thermally induced flow instability.

5.2 THERMALLY INDUCED FLOW STABILITY: ANALYSIS

The flow instability is usually attributed to the Gaussian distribution of CSI on the receiver aperture and is converted to power–on-aperture (PoA), see e.g. [Roldán *et al.*, 2014]. The non-uniform radial heat flux distribution results in a higher temperature of the central absorber than its peripheral counterparts. The same may be exaggerated with a non-uniform heat flux distribution depending on the extinction coefficient as depicted in Chapter 3. Moreover, the thermo-physical property of air such as, kinematic viscosity increases with the temperature, which elevates the flow resistance. As the absorbers are subject to the same pressure-drop, a low mass flow rate ($\dot{m}_a$) of air is expected in the central absorber that may trigger the flow instability. Therefore, the centrally located absorbers are more likely to fail. Ideally the desired equal $\dot{m}_a$ of air through all the pores is to be maintained by a blower. The resulting pressure-drop will be the same across all the absorbers viz. central and peripheral. As already explained, the radial distribution of the concentrated solar irradiance on the receiver aperture is Gaussian in nature, which may lead to the thermally induced flow instability and an unequal $\dot{m}_a$ through the absorber pores. This phenomenon is analyzed with the difference between quadratic pressure at the inlet and outlet of an absorber [Kribus *et al.*, 1996; Pitz-paal *et al.* 1997]. Therefore, a correlation to estimate the pressure-drop across the straight circular pore based absorber is deduced in sub-section 5.1 based on an experiment and the three-dimensional computational fluid dynamics approach. Subsequently, the same is employed for flow-stability analysis in the designed receiver.

Generally, the thermally induced flow instability is analyzed using the quadratic pressure at the inlet and outlet of an absorber [Kribus *et al.*, 1996; Pitz-Paal *et al.*, 1997]. Thus, a correlation is required for estimating the pressure-drop across the designed absorber with straight circular pore. The same is used from eq. (5.2) as follows:

$$\left.\begin{aligned}\Delta p &= K_p \times \frac{\rho_f \mathrm{v}_p^2}{2} \\ K_p &\approx 179.25 Re_p^{-0.588}\end{aligned}\right\} .$$

Where, pressure-drop (Δp) is the same across all the pores of an absorber. Assuming the fully developed laminar flow in an absorber pore or the pressure decreases linearly along the flow direction (z), the pressure-gradient with respect to z, is given by,

$$\frac{dp}{dz} = \frac{\Delta p}{L} = -\frac{179.25 \times Re_p^{-0.588}}{L} . \frac{\rho_f \mathrm{v}_p^2}{2} , \tag{5.7}$$

where, the pore Reynolds number (Re_p), density (ρ_f) and absolute viscosity (μ_f) of air are given by

$$Re_p = \frac{m'' d_p}{\mu_f}, \rho_f = \frac{p}{RT}, \mu_f = \mu_0 \left(\frac{T}{T_0}\right)^{0.7} .$$

Considering that the air temperature attains its maximum (T_{out}) over a few millimeters for a low Re_p it is reasonable to express pressure-drop across a pore as follows:

$$pdp = -\frac{179.25 R \mu_0^{0.588}}{L d_p^{0.588} T_0^{0.412}} . \frac{m''^{1.412}}{2} . T_{out}^{1.412} dz . \tag{5.8}$$

The difference between inlet and outlet quadratic pressure of an absorber is generally employed for flow-stability analysis, see e.g. [Becker *et al.*, 2006]. Integrating eq. (5.8) using $p_{inlet} \leq p \leq p_{outlet}$ and $0 \leq z \leq L$ results in,

$$\Rightarrow p_{inlet}^2 - p_{outlet}^2 = B.(m'' T_{out})^{1.412} \text{ where } B = \left(\frac{179.25 R \mu_0^{0.588}}{d_p^{0.588} T_0^{0.412}}\right), \tag{5.9}$$

where, the mass flux of air (m'') in a clean pore is estimated using the following instantaneous energy balance:

$$\dot{q}_s = \underbrace{m'' A_{pore} c_{pf} (T_{out} - T_0)}_{\text{Rate of convective heat transfer to air}} + \underbrace{\Sigma \sigma A_s (T_s^4 - T_{amb}^4)}_{\substack{\text{Rate of heat loss from inlet surface of absorber material around the pore by radiation}}} + \underbrace{\Sigma \sigma \frac{A_{cs}}{n} (T_{cs}^4 - T_{amb}^4)}_{\substack{\text{Rate of heat loss from surface area of absorber by radiation (equally distributed to } n_p \text{ pores)}}} ,$$

where, A_s and A_{cs} are the cross-section area of absorber material around the pore and circumferential area of the absorber, respectively; A_{pore} is the cross-section area of pore; Σ(=0.6) is the emissivity of absorber material [IRT]; T_0 and T_{amb} are the air temperature- at the pore inlet and of ambient, respectively, with $T_0 \geq T_{amb}$ [Sharma *et al.*, 2015a, 2015b]; T_s and T_{cs} are the average temperature- at the inlet surface of material around a pore and at the absorber circumference, respectively. In this equation, the radiation based heat loss rate from

the circumferential area of absorber is equally redistributed to all the n pores. The convective heat loss is ignored in the analysis. For the maximum value of radiation based heat loss rate, T_{cs} & $T_s \sim T_{out}$ (>>T_{amb}), results in

$$m'' = \frac{q_s'' A_{tot} \Big/ A_{pore} - \Sigma\sigma \left[\left\{ A_s + \left(A_{cs}/n \right) \right\} \Big/ A_{pore} \right] T_{out}^4}{c_{pf}\left(T_{out} - T_0\right)}, \text{ where } \dot{q}_s = q_s'' A_{tot} \text{ with } A_{tot} = A_{pore} + A_s$$

$$\Rightarrow m'' = \frac{q_s'' \Big/ \varepsilon - \Sigma\sigma\beta T_{out}^4}{c_{pf}\left(T_{out} - T_0\right)}, \text{ where } \beta = \left(1 \Big/ \varepsilon - 1 \right) + \frac{A_{cs}}{n A_{pore}} , \tag{5.10}$$

where, β is introduced as a geometry based parameter. By replacing eq. (5.4) in eq. (5.10) the Δp^2 of a pore in an absorber is given by

$$\Delta p^2 = p_{inlet}^2 - p_{outlet}^2 = B'.\left(\frac{q_s'' \Big/ \varepsilon \; T_{out} - \Sigma\beta\sigma T_{out}^5}{\left(T_{out} - T_0\right)} \right)^{1.412} , \text{ where } B' = \frac{B}{c_{pf}^{1.412}} . \tag{5.11}$$

Flow instability is inferred by an unexpected oscillatory nature of Δp^2 with respect to T_{out} beyond a critical heat flux value [Kribus *et al.*, 1996; Pitz-Paal *et al.*, 1997]. It implies a non-unique value of T_{out} at a given Δp^2. This unusual behavior is an indication of flow instability. Such a situation may lead to failure of absorber as a consequence of local hotspots [Hoffschmidt *et al.*, 2003; Fend *et al.*, 2005]. This would imply the existence of a maximum or a minimum satisfying

$$\Rightarrow \; q_s'' = \Sigma\varepsilon\beta\sigma \left(\frac{5T_0 T_{out}^4 - 4T_{out}^5}{T_0} \right) \text{ or } \Sigma\varepsilon\beta\sigma T_{out}^4 . \tag{5.12}$$

The critical or minimum value of heat flux q_s'', if exists at a given T_{out}, beyond which flow instability is expected is calculated using eq. (5.12) as [Becker *et al.*, 2006],

$$\frac{dq_s''}{dT_{out}} = \left| \begin{array}{l} \Sigma\varepsilon\beta\sigma\left(4T_{out}^3\right) \\ or \\ \dfrac{d}{dT_{out}} \left\{ \Sigma\varepsilon\beta\sigma \left(\dfrac{5T_0 T_{out}^4 - 4T_{out}^5}{T_0} \right) \right\} = 0 \;\Rightarrow T_{out}^3 \left(T_0 - T_{out}\right) \end{array} \right\} = 0 ,$$

here, $T_{out} \neq 0$ and therefore the final solution of the above equation becomes,

$$\left.\begin{aligned} &\Rightarrow T_{out} = T_0 \\ &\text{and for the minimum,} \\ &\frac{d^2 q_s''}{dT_{out}^2} > 0 \Rightarrow T_{out} < \frac{3}{4} T_0 \end{aligned}\right\}, \tag{5.13}$$

where, the eq. (5.13) is not feasible as T_{out} >> T_0 and thus, flow instability in the designed open volumetric air receiver is not foreseen under the considered assumptions. This infers the non-existence of such a critical heat flux beyond which flow instability or oscillatory nature of Δp^2 is expected. In other words, a stable operation of the designed receiver with the circular straight pore based cylindrical absorber is envisaged. It must be re-emphasized that the derivation assumes the fully-developed laminar flow in a clean pore, which may be reasonable at a low Re_p. Thus, further assessment of the derived expression for Δp^2 as in eq. (5.5) is required to support the observation. For this purpose, a two-dimensional numerical approach is adopted with a uniform heat flux boundary condition, which is computationally less intensive and is presented in next subsection.

5.2.1 Numerical Simulation and Results

A comparison between the computed and the correlation based Δp is shown in Figure 5.6 with the applied different uniform heat fluxes as boundary conditions up to a Re_p < 300. This shows that (a) the Δp increases and T_{out} decrease with high Re_p, (b) the derived correlation compares within 10-25% with the performed simulations for a T_{out} up to 900 K, covering the range of interest. Thus, the derived correlation for pressure-drop coefficient in eq. (5.2) is realistic and may be used for flow stability analysis at a high temperature and at a low Re_p with the circular straight channel based absorber.

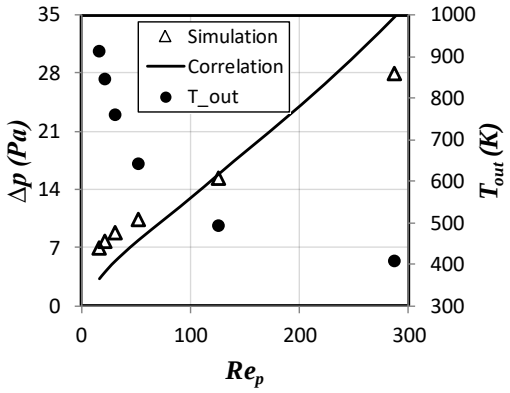

Figure 5.6: Comparison between the derived correlation for pressure-drop at different temperatures.

It is already explained in previous section that Δp^2 across an absorber is employed for the flow-stability analysis. The designed absorber is made of brass and comprise of straight circular pores, as shown in Figure 1.4 (Chapter 1). Assuming an average heat flux on an absorber the two-dimensional axisymmetric single pore model in Fluent with surrounding brass (solid) suffices. Figure 5.7(a) shows the employed structured mesh and the adopted boundary conditions. A uniform heat flux is applied on the circumference of absorber material with 200 ≤ $\dot{q}_s/\dot{m}_a$ (kJ/kg) ≤ 1000. This simulates the volumetric heating effect as reported in the experiments [Sharma *et al.*, 2015a,b]. At the inlet 1.03×10^{-6} ≤ $\dot{m}_a$ (kg/s) ≤ 5.16×10^{-6} is applied and $\dot{q}_s$ is maintained at 1.03 W. The radiation based heat loss at the inlet surface of absorber material is modeled with a user defined function. The natural convection

based loss from absorber is approximately 2-3% of the input power [Sharma *et al.*, 2015b], which is neglected in the presented analysis. The zero gage pressure is applied at the pore outlet. The continuity, momentum and energy equations are solved with the final mesh based on a grid independence test. The validated numerical setup is summarized in the Table 5.4.

Table 5.4: Numerical setup employed for two-dimensional simulations.

Governing Equations	Mesh	Numerical Convergence scheme
Fluid (air) $\nabla \cdot \vec{V} = 0$ $(\vec{V}\cdot\nabla)\vec{V} = -\frac{\nabla p}{\rho} + \nu \nabla^2 \vec{V}$ $\left(\nabla \cdot \rho \vec{V} H\right) = \nabla \cdot \left(\frac{k_f}{c_{pf}} \nabla H_f \right)$ Solid (brass absorber) $\nabla \cdot (k_s \nabla T) = 0$	Structured Resolution: 0.05 mm Maximum aspect ratio: 3.85 Minimum orthogonality: 0.84	First-order 10^{-6} Upwind Algorithm: SIMPLE

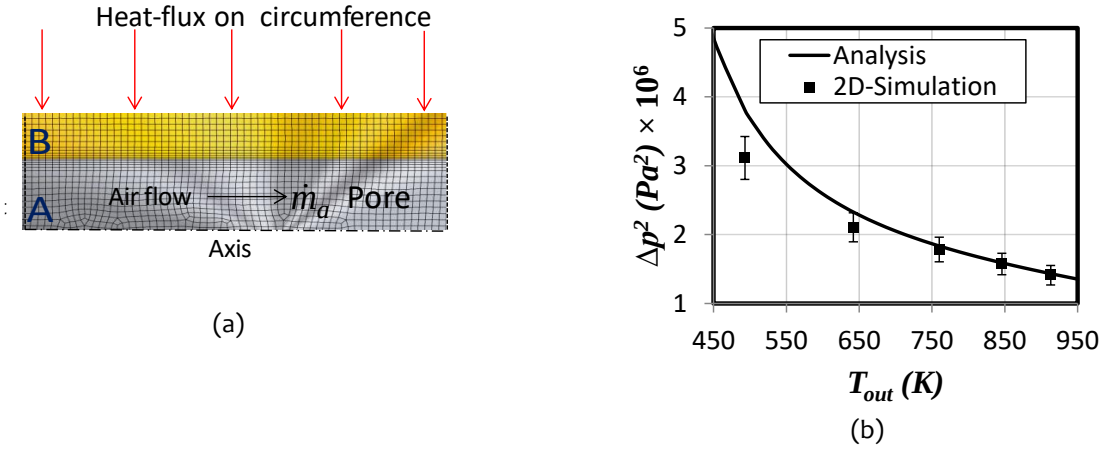

Figure 5.7: (a) A schematic of the employed mesh of two dimensional geometry of single absorber pore (A: Air, B: Brass), (b) A comparison between theoretical and the numerically analyzed values of Δp^2.

Figure 5.7(b) shows a comparison between the theoretical and the computed values of Δp^2. These are plotted against the air temperature at the pore outlet ($T_{out.}$). This illustrates that $\dot{m}_a$ and Δp^2 decrease simultaneously as inferred from the increasing $T_{out.}$. This usual behavior indicates a stable flow regime up to a $\dot{q}_s/\dot{m}_a$ of 1000 kJ/kg [Kribus *et al.*, 1996; Pitz-Paal *et al.*, 1997]. Moreover, the numerically analyzed values of Δp^2 compare well to eq. (5.11) for 400 ≤ $\dot{q}_s/\dot{m}_a$ (kJ/kg) ≤ 1000 within ±10%. Thus, the assumption of constant pressure-gradient is even more appropriate at a low $\dot{m}_a$ or at the critical value of $\dot{q}_s/\dot{m}_a$ ~ 1200 kJ/kg and Re_p ~ O (10), see e.g. [Kribus *et al.*, 1996]. This substantiates the applicability of these approaches and that a stable flow is foreseen in the described receiver. This will be an advantage for operating the innovative solar convective furnace system in which the operating temperature will be limited to 750 K. However, stable flow is envisaged beyond this temperature with an appropriate absorber material.

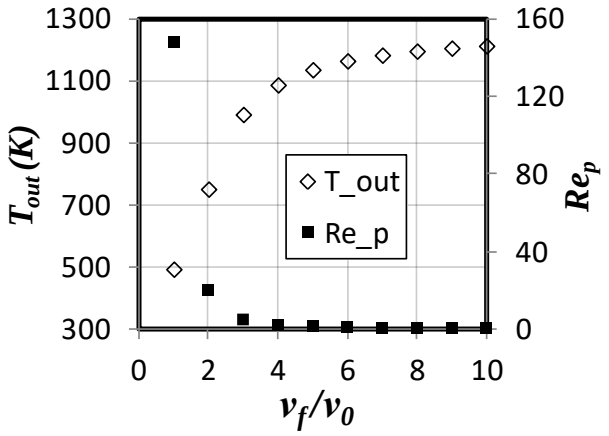

Figure 5.8: Variation of T_{out} and Re_p with the kinematic viscosity ratio of air.

The operating temperature of an open volumetric air receiver exceeds 1200 K [Ávila-Marín, 1996]. The kinematic viscosity of air (υ_f) at this temperature is almost the 10 times that of its reference value (υ_0) at 300 K. With the increasing kinematic viscosity Re_p should decrease owing to flow resistance at a fixed Δp. Therefore, the air temperature at the pore outlet is likely to increase across an absorber. To analyze the same, simulations are performed with a gage total inlet pressure of 15.8 Pa, which corresponds to $\dot{q}_s/\dot{m}_a$ of 200 kJ/kg at 300 K. The kinematic viscosity of air is artificially increased as depicted by υ_f/υ_0 in Figure 5.8, which results in the elevated air temperature at the pore outlet. Consequently, Re_p decreases to $O(1)$ or to a creeping flow, which is favorable to instability [Kribus *et al.*, 1996]. As a consequence, the dust deposition in an absorber pore may trigger flow instability.

5.2.2 Flow Stability: Effect of Dust Deposition

A numerical model is employed and validated with the measured values of T_{out} in the reported experiment with a uniform or volumetric-type heating by Sharma *et al.,* (2015a,b). A variation of the derived expression for Δp^2 with respect to T_{out} for the clean and the partly blocked straight channels with a dust layer thickness up to 200 μm is shown in Figure 5.9. The increment in T_{out} is attributed to the decreasing $\dot{m}_a$ or Δp^2. It is inferred that for a given T_{out}, Δp would then increase with the dust layer thickness, or with the decreasing effective absorber porosity. Also the deposition of dust seems not to promote flow instability in the considered absorber. These observations allow expecting a stable operation of straight pore based open volumetric air receiver in desert regions. This is inferred from Figure 5.9 in which Δp^2 shows a usual behavior as for a stable flow condition in a partially blocked circular straight channel. Moreover, the simulated value of Δp^2 with the uniform dust layer thickness of 100 μm compares well with that of its analyzed values using eq. (5.11), which lends confidence to the numerical results.

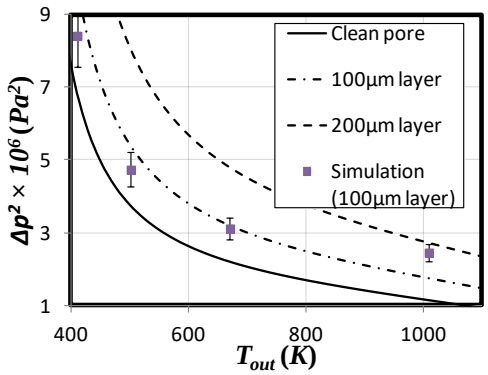

Figure 5.9: Comparison of the analyzed Δp^2 with clean and partly blocked straight channel.

5.3 SUMMARY

The concentrating solar thermal systems based on the open volumetric air receivers allow achieving a temperature beyond 1000 K. These receivers are open to atmosphere that will promote the dust deposition in arid deserts like Rajasthan and the Middle-East. This may lead to its failure and on the other hand the use of a cyclone separator as a cleaning device will enhance the pressure-drop or parasitic loss. To address this issue a correlation for the pressure-drop across the straight pore based cylindrical absorber is derived with an uncertainty of about 10-25 % at a $175 \leq Re_p \leq 600$. Additionally, the available experimental data for various receivers is used to deduce a correlation for the thermal efficiency of an open volumetric air receiver. The limitation of the deduced correlation for thermal efficiency is also discussed. Based on the assessment, the need of additional experiments is concluded. A concept of the efficiency ratio is proposed for addressing the effect of parasitic loss on the performance of an open volumetric air receiver. This analysis clearly demonstrates that (a) the minimum value of power-on-aperture per unit mass-flow-rate should be 200 kJ/kg, (b) the minimum absorber porosity should be 50% and (c) the deposition of dust will reduce the efficiency ratio. Generally, all these requirements are satisfied, however, for mitigating the effect of dust deposition the straight pore based absorbers are recommended.

An open volumetric air receiver should operate at a ratio of power-on-aperture to air mass-flow-rate > 200 kJ/kg. However, at a high heat flux the occurrence of flow instability may be detrimental, which is discussed using theoretical and numerical approach. Analysis of the quadratic pressures difference across the absorber reveals that the designed open volumetric air receiver is not prone to flow instability. This envelopes the targeted air temperature of 750 K for the solar convective furnace and up to a $\dot{q}_s/\dot{m}_a$ of 1000 kJ/kg. This will be an advantage for the envisaged process heat application, namely solar convective furnace. The same is reconfirmed with a two-dimensional numerical simulation having $200 \leq \dot{q}_s/\dot{m}_a$ (kJ/kg) ≤ 1000. However, the presented analysis is based on certain assumptions, which may not be followed by the system in real scenario. Hence, the need of a more detailed analysis is envisaged for the scale-up. As a first step, an unsteady heat transfer model is developed, which includes the effect of return air and is likely to be helpful in identifying important parameters leading to an optimal design. This is presented in Chapter 6.

…